

Strongly bound excitons in gapless two-dimensional structuresYufeng Liang,¹ Ryan Soklaski,¹ Shouting Huang,¹ Matthew W. Graham,² Robin Havener,³ Jiwoong Park,^{4,5} and Li Yang^{1,*}¹*Department of Physics, Washington University in St. Louis, St. Louis, Missouri 63130, USA*²*Laboratory for Atomic and Solid State Physics, Cornell University, Ithaca, New York 14853, USA*³*School of Applied and Engineering Physics, Cornell University, Ithaca, New York 14853, USA*⁴*Department of Chemistry and Chemical Biology, Cornell University, Ithaca, New York 14853, USA*⁵*Kavli Institute at Cornell for Nanoscale Science, Cornell University, Ithaca, New York 14853, USA*

(Received 13 January 2014; published 15 September 2014)

Common wisdom asserts that bound excitons cannot form in high-dimensional ($d > 1$) metallic structures because of their overwhelming screening and the unavoidable resonance with nearby continuous bands. Strikingly we illustrate that this prevalent assumption is not quite true. A key ingredient has been overlooked: Destructive coherent effects are capable of thwarting the formation of resonance. As an example of this general mechanism, we focus on an experimentally relevant material and predict bound excitons in twisted bilayer graphene, which is a two-dimensional gapless structure that exhibits metallic screening. The binding energies calculated by first-principles simulations are surprisingly large. The low-energy effective model reveals that these bound states are produced by a unique destructive coherence between two alike subband resonant excitons. In particular, this coherent effect is not sensitive to the screening and dimensionality, and hence may persist as a general mechanism for creating bound excitons in various metallic structures, opening the door for excitonic applications based on metallic structures.

DOI: [10.1103/PhysRevB.90.115418](https://doi.org/10.1103/PhysRevB.90.115418)

PACS number(s): 78.67.Wj, 71.15.-m, 71.35.-y, 81.05.ue

I. INTRODUCTION

Bound excitons, electron-hole (e-h) pairs, are of great interest because of their neat physics picture and their long lifetimes, which make them viable for broad applications, including photovoltaics and photocatalytics [1–3]. However, the formation of bound e-h pairs had been thought to be impossible in metallic (gapless) systems due to their overwhelming screening effects. Moreover, e-h pairs in gapless structures tend to hybridize with continuous transitions nearby, forming resonant states, whose intrinsic lifetime is substantially diminished. To date, the only exception was found in metallic carbon nanotubes (mCNTs), in which the depressed one-dimensional (1D) screening together with the unique optical symmetry gap led to the formation of a bound e-h pair [4–8]. These studies raised many obvious but fundamental questions: besides 1D metals, can bound excitons be observed in structures with stronger dielectric screening, e.g., higher dimensional ($d > 2$) gapless materials? In addition to the symmetry-related reason revealed in mCNTs, are there any other mechanisms responsible for the formation of bound excitons in gapless systems?

Graphene, a two-dimensional (2D) semimetal, may serve as an excellent testbed for answering these outstanding questions. Unfortunately, due to broad Fano resonance effects [9–12], no evidence of bound excitons has been observed in graphene, despite the presence of significant e-h interactions. Recently, twisted bilayer graphene (tBLG) [13–22], a 2D semimetal, has garnered substantial interest in its optical properties, since a twist between graphene sheets introduces new van Hove singularities (vHSs) [13, 16, 17] that emerge at the intersections of Dirac cones on opposite layers. From the perspective of excitons, this unique band structure with several vHSs (see

Fig. 1) has a particular implication for unusual excitonic effects. As shown in Figs. 1(b) and 1(c), the outlined bands in each schematic are parallel to each other, due to the proximate group velocities of electrons and holes, which lead to a large joint density of states (JDOS). This special band topology enhances e-h interactions and therefore sheds new light on the potential existence of bound e-h pairs in 2D metallic systems.

In this work we predict the existence of strongly bound excitons in higher-dimensional gapless structures by a new destructive coherent effect, the ghost Fano resonance. As an example of realistic material, we focus on excitonic effects of tBLG. Through first-principles *GW*-Bethe Salpeter Equation (BSE) simulations, we successfully observe a bound (though less bright) exciton with a significant binding energy of 0.5 eV in tBLG, which is an order of magnitude larger than that found in mCNTs [3–6] and is even comparable to those in semiconducting nanostructures [4, 5, 23–27]. With the help of the low-energy effective model, we found that the formation of this unusual bound exciton is explained by the ghost Fano resonance [28, 29], a unique destructive coherence between two sets of resonant states with similar energies. This represents a new mechanism for forming bound excitons in gapless systems. In particular, because of its coherent origin, our proposed mechanism gives hope to a general mechanism for creating bound excitons in many other metallic systems with double resonance, despite their strong screening.

The paper is organized as follows.

II. OPTICAL ABSORPTION SPECTRA OF tBLG

We perform first-principles calculations by employing the many-body Green's function theory for tBLG. We focus on two commensurate structures [15] with 21.8° and 32.2° rotated from the AB-stacking order. Our study begins with a density-functional-theory (DFT) calculation within the local density

*lyang@physics.wustl.edu

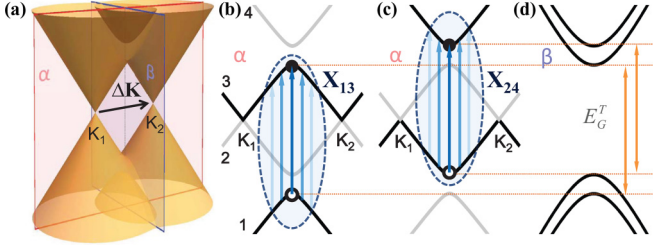


FIG. 1. (Color online) (a) Low-energy band structure of tBLG. α (light red) is the plane passing both axes of the Dirac cones, whereas β (light blue) is the bisector plane of the two cones. (b) and (c) Schematic formation of exciton X_{13} (b) and X_{24} (c) illustrated on the α plane. The energy bands are labeled with 1 to 4 in ascending energy order. The involved bands are outlined in black, while the states that mainly compose the exciton are enclosed by the ellipses. (d) Bands plotted on the β plane. $E_G^T = \hbar v_F |\Delta \mathbf{K}|$ is the transition energy gap between the first (second) and third (fourth) band.

approximation (LDA) [30]. Next, the dielectric function is calculated using the random-phase approximation with a $30 \times 30 \times 1$ ($18 \times 18 \times 1$) \mathbf{k} grid [31] over the first Brillouin zone. Meanwhile a slab-Coulomb-truncation scheme [32] is also employed. We then obtain the quasiparticle (QP) band energies within the G_0W_0 approximation [33]. The vital step in describing the many-body excitonic effects is to solve the BSE [34]:

$$(E_{c\mathbf{k}} - E_{v\mathbf{k}})A_{v\mathbf{c}\mathbf{k}}^S + \sum_{v'\mathbf{c}'\mathbf{k}'} \langle v\mathbf{c}\mathbf{k} | K^{\text{eh}} | v'\mathbf{c}'\mathbf{k}' \rangle A_{v'\mathbf{c}'\mathbf{k}'}^S = \Omega^S A_{v\mathbf{c}\mathbf{k}}^S, \quad (1)$$

where $A_{v\mathbf{c}\mathbf{k}}^S$ is the exciton wave function in \mathbf{k} space, Ω^S is the exciton eigenenergy, K^{eh} is the e-h interaction kernel, and $|v\mathbf{k}\rangle$ and $|c\mathbf{k}\rangle$ are the hole and electron states, respectively [34]. To ensure a smooth and accurate optical spectrum, we incorporated a fine $60 \times 60 \times 1$ ($36 \times 36 \times 1$) \mathbf{k} grid in solving the BSE. Seven (12) valence bands and seven (12) conduction bands are included to cover a broad range of the optical absorption spectrum up to 6.0 eV.

Both optical spectra with and without e-h interactions are presented in Figs. 2(a) and 2(b) with three distinct peaks (marked by E_1 , E_2 , and E_3 in noninteracting spectra). Our calculation yields an excellent agreement with our recent optical conductivity measurements [19,20]; the first two peaks, E_1 and E_2 , stem from the two intersections between the Dirac cones from opposite layers, and the third one, E_3 , results from the perturbed saddle-point vHSs intrinsic to monolayer graphene [18,19]. We observe enhanced excitonic effects in the absorbance. e-h interactions cause peaks E_1 and E_2 to redshift by ~ 0.2 eV for both twist angles.

III. BOUND EXCITONS IN tBLG

The fundamental mechanism forming the corresponding excitonic states in these new prominent peaks in tBLG (E_1 and E_2), however, may be substantially different from our knowledge learned from usual BLG [11,35]. At the band intersection between two Dirac cones, only two sets of optical transitions with similar energies are allowed due to the selection rule, as shown in Figs. 1(b) and 1(c), producing double resonance [16,17]. From the point view of two-particle excitations, the parallel sets of bands give

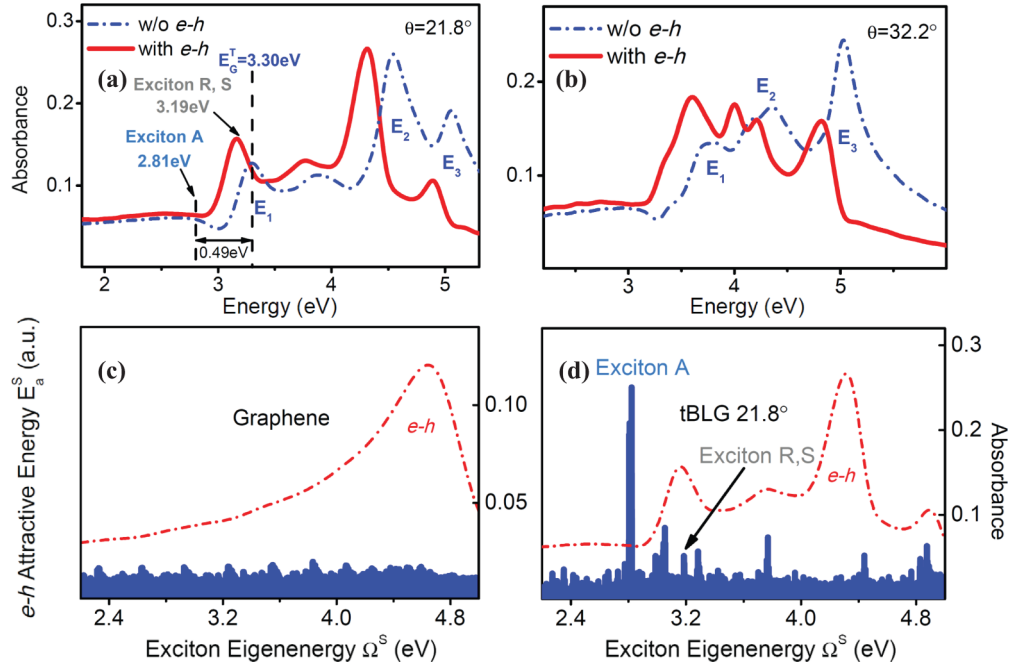


FIG. 2. (Color online) (a) and (b) Optical absorbance obtained by the $GW + \text{BSE}$ method. The blue dash-dotted curves are the noninteracting spectra, while the red solid ones are the spectra with the e-h interactions included. (c) and (d) e-h attractive energy E_a^S (blue bars, in arbitrary unit) plotted versus the exciton energy Ω^S for graphene (c) and tBLG (d) within an identical energy window from 2.2 to 5.0 eV, where those unusual excitonic effects happen. For references, the absorbance spectra of both structures are also plotted (red dashed curves).

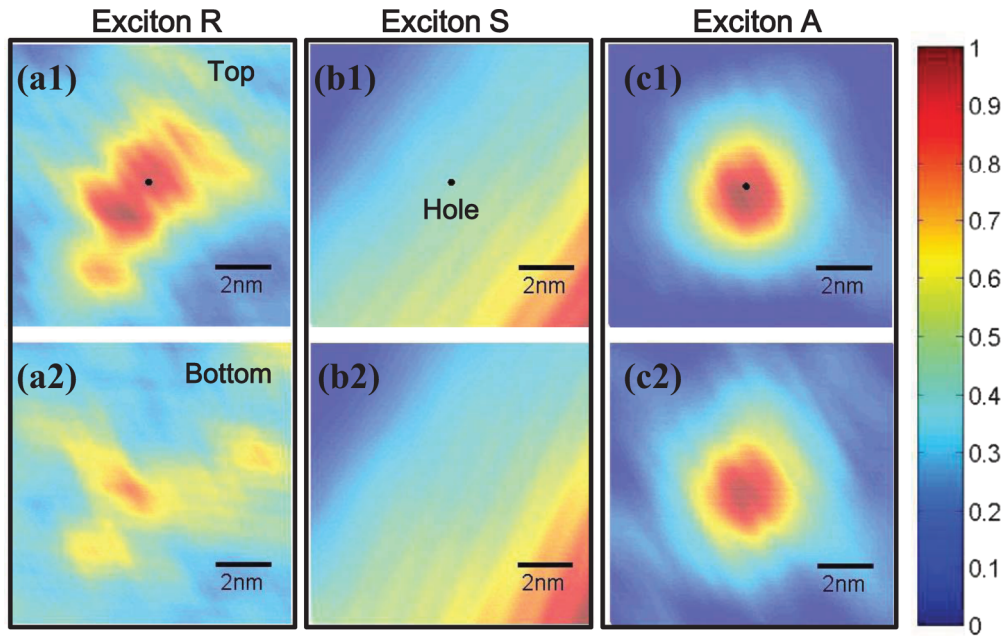


FIG. 3. (Color online) $|\chi_S(\mathbf{x}_e, \mathbf{x}_h)|^2$ of excitons R , S , and A in 21.8° tBLG plotted on the top layer (a1)–(c1) and the bottom layer (a2)–(c2) with the hole fixed at the most-probable position on the top sheet. The distribution of the electron is normalized to the maximal probability of the two layers so that it ranges from 0 (blue) to 1 (red). The details within the primitive cell are less important and thus have been smoothed out.

rise to significant JDOS and potentially unusual bound e-h pairs.

The most direct approach to examine whether an excitonic state is bound or resonant is to investigate its wave function in real space. We plot the wave functions of two typical bright excitons, R and S , located around peak E_1 [marked in Fig. 2(a)]. Here R is the brightest excitonic state around the absorption peak. However, as shown in Figs. 3(a) and 3(b), the electron is distributed loosely around the hole and even extends beyond our simulation range. These wave functions manifest a signature of resonant states, as observed in graphene [11] and CNTs [4–6]; the binding feature of excitons is substantially weakened by hybridization with continuous Bloch states that are spatially periodic and extended. In conclusion, these prominent peaks in Fig. 2 are dominated by resonant excitons, instead of bound ones.

So far we have focused on the brightest exciton, which often corresponds to the most bound state. However, bound states are not necessarily bright [36]. In order to find possible bound exciton states that are not optically active, we have to, in principle, scan all excitonic states solved by BSE and inspect their real-space wave functions, which is implausible because of a huge number of excitonic states (more than 170 000). Motivated by the fact that e-h interactions of bound excitons are typically more significant than those of resonant ones, we evaluate the e-h attractive energy for a given excitonic state S , by calculating E_a^S , expectation value of the e-h interaction kernel K^{eh} sandwiched by that state $|S\rangle$:

$$E_a^S = \langle S | K^{\text{eh}} | S \rangle = \sum_{v\mathbf{ck}} (E_{c\mathbf{k}} - E_{v\mathbf{k}}) |A_{v\mathbf{ck}}^S|^2 - \Omega^S. \quad (2)$$

E_a^S is not the binding energy, but it can be understood as the difference between the exciton's "kinetic energy" and its eigenenergy, roughly reflecting the degree of e-h attractions.

As seen in Eq. (2), the kinetic energy term is the net kinetic energy of excitons plus the weighted single-particle band energy difference between electrons and holes.

Using this e-h attractive energy analysis, an intriguing comparison can be made between monolayer graphene and tBLG. For both cases, we plot the e-h attractive energy spectra (E_a^S versus Ω^S) for all exciton states in Figs. 2(c) and 2(d). Surprisingly, the E_a^S spectrum of graphene [see the blue-bar plot in Fig. 2(c)] exhibits no distinct features up to 5.0 eV, even for the prominent absorption peak at 4.6 eV. This indicates that all its excitonic states are broadly resonant [11]; however, the E_a^S spectrum of tBLG [Fig. 2(d)] clearly shows several distinct spikes over a broad energy range, implying the existence of excitonic states with stronger e-h interactions. Following this idea, we select the most bound excitonic state A [marked by an arrow in Fig. 2(d)] and plot its real-space wave function in Figs. 3(c1) and 3(c2). For this case we obtain an isotropic distribution with significant localization. Our calculation predicts the presence of a bound exciton state in tBLG, a 2D gapless material.

More questions are raised regarding exciton A . First, its energy is not at the prominent absorption peak (E_1) but approximately 0.38 eV below it. Moreover, its optical oscillator strength is weak, roughly one fifth of that of brightest excitonic state R . These are in conflict with the conventional wisdom; the most bound state is usually the most optically active one according to the hydrogen model. Second, since the position of the peak E_1 in the noninteracting spectrum indicates the transition energy E_G^T between the valence and conduction vHSs, the bound exciton A emerges 0.49 eV below the E_G^T in Fig. 2(a). Such a surprisingly large binding energy (~ 0.5 eV) is an order of magnitude larger than that found in mCNTs [4–6] and it is even comparable to those exciton binding energies of semiconducting nanostructures [4,5,23–27].

IV. LOW-ENERGY EFFECTIVE MODEL

Unfortunately, it is challenging to directly analyze the results of our above first-principles simulation. Here we use a low-energy effective model [22] for simplifying the analysis:

$$H(\mathbf{k}) = \begin{pmatrix} H_0(\mathbf{k}, 0) & T^+ \\ T & H_0(\mathbf{k} - \Delta\mathbf{K}, \theta) \end{pmatrix}, \quad (3)$$

where the intralayer dispersion and the interlayer interaction are, respectively,

$$H_0(\mathbf{k}, \theta) = \hbar v_F \begin{pmatrix} 0 & e^{-i\theta}(k_x - ik_y) \\ e^{i\theta}(k_x + ik_y) & 0 \end{pmatrix},$$

$$T = \Delta \begin{pmatrix} 0 & 1 \\ 1 & 0 \end{pmatrix}.$$

The matrix T describes the average interlayer interaction between AB and BA stacking order, where Δ is the interlayer coupling strength. We approximate the screened Coulomb interaction in the direct term K_d^{ch} with the 2D Coulomb potential $v_c(q) \propto 1/q$ but drop the exchange term K_x^{ch} because of its lessened importance in the graphene-related systems [37]. With the model we then solve the BSE on a uniform \mathbf{k} grid with approximately 2000 k points in proximity of the two Dirac cones. As an example, we choose a tBLG with 5° rotation with interlayer coupling strength Δ of 130 meV. It has to be pointed out that this low-energy effective model is best for small-twisting angles because the linear Dirac-Fermion dispersion is excellently preserved there.

Following the analysis via Eq. (2), we scan the e-h attractive energy spectrum obtained by our model BSE calculations. Now, the transition energy gap E_G^T is 1.05 eV and we focus on the energy regime below it. Interestingly, as displayed in Fig. 4(a), a series of discrete excitonic states $X_n (n = 1, 2, \dots)$ are found with distinct e-h attractive energies E_a^S alongside a background of resonant excitons (marked by gray bars) because of enhanced e-h interactions. With ascending exciton

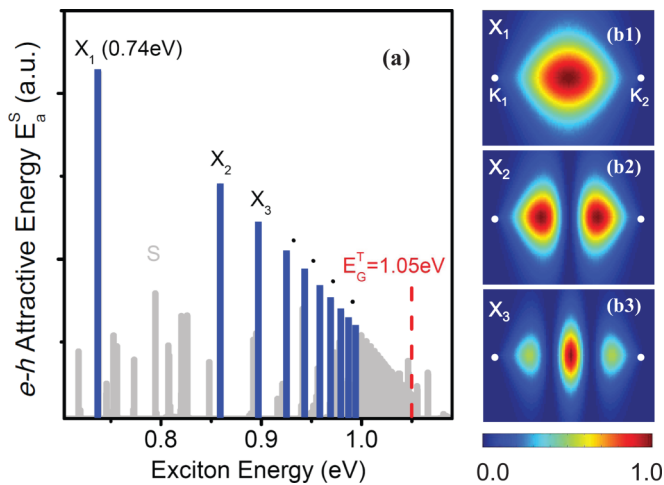


FIG. 4. (Color online) (a) e-h attractive energy from the low-energy effective model. The blue bars mark the exciton states with prominent e-h attractive energies, whereas the gray bars represent the background states of less interest. (b1)–(b3) Modulus squared wave function of exciton X_1 , X_2 , and X_3 .

energy, their population becomes denser towards E_G^T , whereas E_a^S decreases monotonically. If E_G^T and E_a^S are regarded as a “band gap” and “binding energies,” respectively, they exhibit standard features of bound excitons in semiconductors. In particular, we have plotted envelop wave functions of the lowest few states X_n in the reciprocal space, as shown in Fig. 4(b). We immediately see their bound-state nature. For example, the distribution of X_1 is highly analogous to $1s$ state of hydrogen. Also given the fact that X_1 possesses the largest e-h attractive energy, we can conclude X_1 corresponds to exciton A in our first-principles simulations.

To further explain why we have bound excitons X_n in tBLG, we investigate their origins. Strikingly we find that each state X_n is only composed of two branches of double-resonant transitions ($1 \rightarrow 3$ and $2 \rightarrow 4$), indicating that it is free of resonance with the Dirac continuum transition ($2 \rightarrow 3$) occurring at low energies.

The above observation also inspires us to further investigate the relation of X_n to the excitonic states solved on the $1 \rightarrow 3$ and $2 \rightarrow 4$ transition subspaces, for which we respectively obtain a set of subband bound excitons $X_{13,n}$ [Fig. 1(b)] and $X_{24,n}$ [Fig. 1(c)], emerging at identical energies $\Omega^{X_{13,n}} = \Omega^{X_{24,n}}$. Surprisingly, for each n , we find that the state X_n are in fact purely antisymmetric superposition of two subspace excitons $X_{13,n}$ and $X_{24,n}$,

$$|X_n\rangle = \frac{1}{\sqrt{2}}(|X_{13,n}\rangle - |X_{24,n}\rangle). \quad (4)$$

Because of the antiphase coherence, the optical oscillator strength of X_n is diminished. On the other hand, the symmetrically superposed states between $X_{13,n}$ and $X_{24,n}$ contribute to a set of higher-energy states, which are resonant and bright excitons. This understanding can be evidenced by Fig. 5(a), in which we present the projected density of states (PDOS) of the subband exciton $X_{13,1}$ (or $X_{24,1}$) over the full space $\{X_f\}$. Both $X_{13,1}$ and $X_{24,1}$ found near 0.78 eV have 50% overlap with X_1 occurring around 0.74 eV, which is seen as a single spike in the PDOS. Meanwhile, they overlap with a number of excitonic states at higher energy (around $\Omega^1 = 0.82$ eV), suggesting they have resonant components there. Moreover, although the oscillator strengths of $X_{13,n}$ and $X_{24,n}$ are individually bright, the destructive interference of the two components in exciton

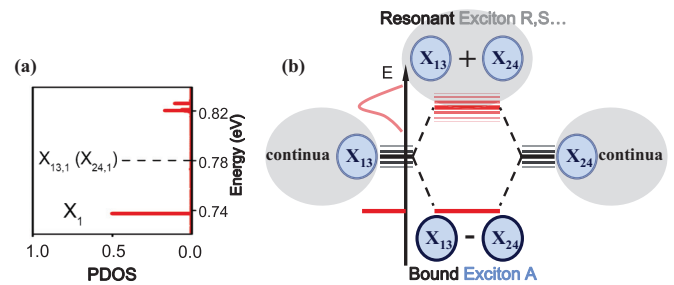


FIG. 5. (Color online) (a) PDOS $|\langle X_{13,1} | X_f \rangle|^2$ ($|\langle X_{24,1} | X_f \rangle|^2$) where X_f goes over the full exciton space. (b) Exciton hybridization diagram in tBLG. The outlined circles represent the excitons formed on either the $1 \rightarrow 3$ or $2 \rightarrow 4$ transition subspaces, while the gray ellipses represent the continua. The plus (minus) sign indicates the symmetric (antisymmetric) superposition of exciton states.

A renders its net oscillator strength relatively weak compared to the optically active higher-energy excitons, such as R and S .

In summary, the model calculation provides a surprising picture of excitonic interference as displayed in Fig. 5(b), in analogy with the so-called ghost Fano resonance discovered in the model of quantum dot molecules [28,29], in which the coherent effects between two similar-energy fano resonances give rise to a nonresonant energy level. First, although subband excitons $X_{13,n}$ and $X_{24,n}$ might hybridize with those $1 \rightarrow 4$ and $2 \rightarrow 3$ transition continua, they are also subject to mutual hybridization and are thrown into a symmetric state and an antisymmetric one. In the symmetric state, the coupling of $X_{13,n}$ and $X_{24,n}$ with the two transition continua interfere *constructively*, broadening into a group of bright excitonic states at higher energies via a conventional Fano resonance, as evidenced by the resonant components near 0.82 eV in the model. Meanwhile, in the antisymmetric state, the couplings with the two continua cancel each other, resulting in a dark and localized state X_n at lower energy via the ghost Fano resonance [28], as evidenced by the sharp spike at 0.74 eV in the model. Compared with e-h interactions, this resonant effect is a higher-order correction and the energy splitting is only 0.08 eV.

We note that the above model is appropriate for small twist angle, and it may not be fully compatible with the quantitative results of our first-principles simulation, in which the twist angles are large (21.8° and 32.2°). However, the essential physics, such as the double resonance of transitions and the related destructive interference, should still play an important role in shaping the strongly bound exciton A , even though the imperfect symmetry of conduction and valence bands could weaken the deconstructive effect, making exciton A not completely dark and not perfectly bound. *Therefore, the above model results depend on the double resonance picture but are not sensitive to the twisting angle.* Our predicted bound excitons shall widely exist in tBLG and even other twisted 2D structures.

V. DISCUSSIONS

Finally, our predicted bound excitons will result in important experimental observations. For example, we expect the

lifetime of optical excitations in tBLG will be much longer than that in graphene and BLG; the corresponding decay of optical currents shall reflect this effect. Moreover, two-photon techniques or applying magnetic field may provide a means to detect them, as what had been done to observe dark excitons in CNTs [38,39]. In particular, the double-resonant picture holds better for tBLG with small twist angles because of the better e-h band symmetry. Therefore, we expect the lifetime of these bound excitons will become longer as the twist angle is reduced. More importantly, this formation mechanism is a coherent effect that is not strongly affected by the screening and e-h interaction strength. Therefore, we expect this phenomenon to be robust in many metallic systems and, particularly, those twisted 2D structures.

VI. SUMMARY

In conclusion, we have demonstrated a mechanism for the formation of strongly bound excitons in 2D (semi) metallic nanostructures via the decoherent effect, the ghost Fano resonance. A strongly bound exciton with a 0.5 eV binding energy is identified in tBLG, which is an order of magnitude than the previous one identified in mCNTs. More importantly, our predicted mechanism for forming strongly bound excitons is not sensitive to the screening and dimensionality, and hence may persist as a general mechanism for creating bound excitons in metallic structures. Therefore, this gives rise to room-temperature excitonic applications based on 2D and even higher-dimensional metallic structure.

ACKNOWLEDGMENTS

This work is supported by the National Science Foundation Grant No. DMR-1207141 and by the Air Force Office of Scientific Research (FA9550-09-1-0691 and FA9550-10-1-0410). The computational resources have been provided by the Lonestar of Teragrid at the Texas Advanced Computing Center (TACC). The DFT calculation is performed with the Quantum Espresso [40], while the GW-BSE calculation is done with the BerkeleyGW package [41].

-
- [1] Y. Cao, I. D. Parker, G. Yu, C. Zhang, and A. J. Heeger, *Nature (London)* **397**, 414 (1999).
 - [2] F. Wang, G. Dukovic, L. E. Brus, and T. F. Heinz, *Science* **308**, 838 (2005).
 - [3] P. Avouris, M. Freitag, and V. Perebeinos, *Nat. Photon.* **2**, 341 (2008).
 - [4] C. D. Spataru, S. Ismail-Beigi, L. X. Benedict, and S. G. Louie, *Phys. Rev. Lett.* **92**, 077402 (2004).
 - [5] C. D. Spataru, S. Ismail-Beigi, L. X. Benedict, and S. G. Louie, *Appl. Phys. A* **78**, 1129 (2004).
 - [6] J. Deslippe, C. D. Spataru, D. Prendergast, and S. G. Louie, *Nano Lett.* **7**, 1626 (2007).
 - [7] F. Wang, D. J. Cho, B. Kessler, J. Deslippe, P. J. Schuck, S. G. Louie, A. Zettl, T. F. Heinz, and Y. R. Shen, *Phys. Rev. Lett.* **99**, 227401 (2007).
 - [8] E. Malic, J. Maultzsch, S. Reich, and A. Knorr, *Phys. Rev. B* **82**, 035433 (2010).
 - [9] K. F. Mak, J. Shan, and T. F. Heinz, *Phys. Rev. Lett.* **106**, 046401 (2011).
 - [10] D. H. Chae, T. Utiakl, S. Weisenburger, H. Giessen, K. Klitzing, M. Lippitz, and J. Smet, *Nano Lett.* **11**, 1379 (2011).
 - [11] L. Yang, J. Deslippe, C. H. Park, M. L. Cohen, and S. G. Louie, *Phys. Rev. Lett.* **103**, 186802 (2009).
 - [12] U. Fano, *Phys. Rev.* **124**, 1866 (1961).
 - [13] G. Li, A. Luican, J. dos Santos, A. Neto, A. Reina, J. Kong, and E. Andrei, *Nat. Phys.* **6**, 109 (2010).
 - [14] E. Mele, *Phys. Rev. B* **81**, 161405 (2010).
 - [15] J. M. B. Lopes dos Santos, N. M. R. Peres, and A. H. Castro Neto, *Phys. Rev. Lett.* **99**, 256802 (2007).

- [16] Z. Ni, L. Liu, Y. Wang, Z. Zheng, L. J. Li, T. Yu, and Z. Shen, *Phys. Rev. B* **80**, 125404 (2009).
- [17] R. W. Havener, H. Zhuang, L. Brown, R. G. Henning, and J. Park, *Nano Lett.* **12**, 3162 (2012).
- [18] P. Moon and M. Koshino, *Phys. Rev. B* **87**, 205404 (2013).
- [19] R. W. Havener, Y. Liang, L. Brown, L. Yang, and J. Park, *Nano Lett.* **14**, 3353 (2014).
- [20] Y. Wang, Z. Ni, L. Liu, Y. Liu, C. Cong, T. Xu, X. Wang, D. Shen, and Z. Shen, *ACS Nano* **4**, 4074 (2010).
- [21] Z. Chen and X. Q. Wang, *Phys. Rev. B* **83**, 081405 (2011).
- [22] E. J. Mele, *Phys. Rev. B* **84**, 235439 (2011).
- [23] L. Yang, M. L. Cohen, and S. G. Louie, *Nano Lett.* **7**, 3112 (2007).
- [24] D. Prezzi, D. Varsano, A. Ruini, A. Marini, and E. Molinari, *Phys. Rev. B* **77**, 041404(R) (2008).
- [25] C. H. Park, C. D. Spataru, and S. G. Louie, *Phys. Rev. Lett.* **96**, 126105 (2006).
- [26] L. Yang, C. D. Spataru, S. G. Louie, and M. Y. Chou, *Phys. Rev. B* **75**, 201304 (2007).
- [27] M. Bruno, M. Palummo, A. Marini, R. D. Sole, V. Olevano, A. N. Kholod, and S. Ossicini, *Phys. Rev. B* **72**, 153310 (2005).
- [28] M. L. Ladron de Guevara, F. Claro, and P. A. Orellana, *Phys. Rev. B* **67**, 195335 (2003).
- [29] H. Lu, R. Lu, and B. Zhu, *Phys. Rev. B* **71**, 235320 (2005).
- [30] W. Kohn and L. Sham, *Phys. Rev.* **140**, A1133 (1965).
- [31] For the dielectric function, the \mathbf{k} grid for tBLG is equivalent to a $80 \times 80 \times 1$ ($30\sqrt{28/4} \approx$) \mathbf{k} grid for the Bernal-stacking graphene which contains four atoms in a primitive cell, compared with the $64 \times 64 \times 1$ in the previous study [8]. For solving the BSE, our \mathbf{k} grid is equivalent to $160 \times 160 \times 1$, compared with the previous $128 \times 128 \times 1$.
- [32] S. Ismail-Beigi, *Phys. Rev. B* **73**, 233103 (2006).
- [33] M. S. Hybertsen and S. G. Louie, *Phys. Rev. B* **34**, 5390 (1986).
- [34] M. Rohlfing and S. G. Louie, *Phys. Rev. B* **62**, 4927 (2000).
- [35] L. Yang, *Phys. Rev. B* **83**, 085405 (2011).
- [36] R. Matsunaga, K. Matsuda, and Y. Kanemitsu, *Phys. Rev. Lett.* **101**, 147404 (2008).
- [37] C. H. Park and S. G. Louie, *Nano Lett.* **10**, 426 (2010).
- [38] A. Srivastava, H. Htoon, V. I. Klimov, and J. Kono, *Phys. Rev. Lett.* **101**, 087402 (2008).
- [39] Y. Piao, B. Meany, L. R. Powell, N. Valley, H. Kwon, G. C. Schatz, and Y. Wang, *Nat. Chem.* **5**, 840 (2013).
- [40] P. Giannozzi *et al.*, *J. Phys.: Condens. Matter* **21**, 395502 (2009).
- [41] J. Deslippe, G. Samsonidze, D. A. Strubbe, M. Jain, M. L. Cohen, and S. G. Louie, *Comput. Phys. Commun.* **183**, 1269 (2012).